Analytical study of fundamental oscillation frequencies around black holes in nonlocal gravity

Rana Muhammad Zulqarnain[1†] Phongpichit Channuie[2,3‡] Abdelmalek Bouzenada[4§] Asifa Ashraf[5,6♮] Farruh Atamurotov[7♯] Ikhtiyor Saidov[8,9¶]

[1]School of Business, Xian International University, Xi'an 710077, China
[2]School of Science, Walailak University, Nakhon Si Thammarat 80160, Thailand
[3]College of Graduate Studies, Walailak University, Nakhon Si Thammarat 80160, Thailand
[4]Laboratory of Theoretical and Applied Physics, Echahid Cheikh Larbi Tebessi University, Bir El Ater 12001, Algeria
[5]School of Physics, Harbin Institute of Technology, Harbin 150001, China
[6]Research Center of Astrophysics and Cosmology, Khazar University, Baku AZ1096, Azerbaijan
[7]Kimyo International University in Tashkent, Tashkent 100121, Uzbekistan
[8]Tashkent State Technical University, Tashkent 100095, Uzbekistan
[9]University of Tashkent for Applied Sciences, Tashkent 100149, Uzbekistan

Abstract: In this study, we investigate the dynamics of test particles in the spacetime of a static, spherically symmetric black hole (BH) illustrated within nonlocal gravity models. After presenting the BH geometries and horizon structures, we examine the motion of particles by analyzing the effective potential, innermost stable circular orbits, and corresponding effective force. We then extend the study to small perturbations of circular orbits, exploring harmonic oscillations characterized by frequencies measured by both local and distant observers, as well as the periastron precession effects. Particular attention is given to the interplay between the nonlocal gravity corrections and the stability properties of geodesics. We analyze the center-of-mass energy of colliding particles near the event horizon and show the influence of BH parameters on energy extraction processes. The results show the mechanism of influnece of nonlocal modifications of gravity on the standard predictions of the BH structure, orbital stability, and high-energy particle dynamics, with possible implications for astrophysical observations and theoretical models of strong gravity. This study examines the differences between the inverse electrodynamics of BHs and the Schwarzschild BH configuration, demonstrating the influnece of additional parameters on the dynamics and stability of test particles.

Keywords: nonlocal gravity, black hole spacetime, particle dynamics, stable circular orbits, harmonic oscillations, center-of-mass energy

DOI: 10.1088/1674-1137/ae432c **CSTR:** 32044.14.ChinesePhysicsC.50065104

I. INTRODUCTION

In 2019, the Event Horizon Telescope (EHT) collaboration [1−6] achieved a groundbreaking milestone in astronomy by presenting the first direct image of a black hole (BH), almost exactly a century after the famous 1919 solar eclipse experiment that confirmed Einstein's prediction of light deflection. This discovery provided compelling observational evidence for one of the most intriguing features of general relativity (GR): photons traveling in the extreme curvature of spacetime near a BH can experience enormous deflections, and in some cases may even orbit the BH on unstable circular-photon trajectories. Because no light escapes from within the horizon, such behavior produces a striking observational signature, namely, a dark central region surrounded by a luminous ring of radiation emitted by infalling matter known as the BH shadow. The concept that this shadow could actually be resolved was first put forward by Falcke et al. [7] and developed further by Melia and Falcke [8], who used numerical simulations to argue that very long baseline interferometry (VLBI) at millimeter

Received 21 November 2025; Accepted 9 February 2026; Accepted manuscript online 10 February 2026

† E-mail: ranazulqarnain7777@gmail.com
‡ E-mail: phongpichit.ch@mail.wu.ac.th (Corresponding author)
§ E-mail: abdelmalekbouzenada@gmail.com
♮ E-mail: asifamustafa3828@gmail.com
♯ E-mail: atamurotov@yahoo.com
¶ E-mail: ixti06.27@gmail.com

wavelengths could achieve sufficient angular resolution to detect the shadow of the supermassive BH at our galactic center, Sagittarius A^* [9−17]. Their calculations predicted an angular size of approximately 30μ, with later refinements of mass and distance measurements updated to approximately 54μ, precisely within the resolving power of a coordinated Earth-sized VLBI array. Realistic modeling based on general-relativistic magnetohydrodynamics [18−22] explored the influence of accretion physics, magnetic fields, and radiative processes on the appearance of Sagittarius A^* and similar objects. Although Sagittarius A^* remained a prime target, the EHT first succeeded in imaging a supermassive BH in galaxy M87 owing to its immense mass and greater brightness at millimeter wavelengths. The success of this effort depended not only on extraordinary technological innovations, combining radio telescopes worldwide to create an effective Earth-sized aperture but also on advanced computational algorithms capable of reconstructing coherent images from sparse interferometric data. The resulting image [23−29] revealed the expected bright ring that encloses a dark interior, a clear manifestation of the predicted shadow. Beyond being a historic achievement, this result began a new era in BH astrophysics [30−44]. Other shadow studies now aim to extract information regarding the mass, spin, and orientation of BHs and probe the role of plasma dynamics, accretion physics, jet launching, and even possible deviations from Einstein's theory of gravity [45−64]. The observational realization of BH shadows has established a transformative tool for investigating gravity in its most extreme regime, deepening our understanding of the very fabric of spacetime itself [23−29].

The nonlocal gravity framework [65–66] illustrates a significant development in modern gravitational physics, proposing modifications to GR in which the behavior of spacetime is not illustrated solely by local curvature $(\alpha \neq 0)$ but instead influenced by these nonlocal contributions across the manifold [67–68]. This broader perspective gives new information for reconciling long-standing challenges in cosmology and astrophysics, and presents new explanations that extend beyond the limits of classical Einstein gravity [69–70]. Nonlocal gravity has been identified as a promising approach to resolve issues such as BH singularities, the inflationary phase of the early universe, the enigmatic nature of dark energy, and the dynamics of large-scale structure formation [71–72]. By abandoning the strict principle of locality, these models bypass the typical instabilities associated with higher-derivative operators in ultraviolet corrections of Einstein's theory, producing effective Lagrangians that are renormalizable and consistent with the kind of nonlocal contributions expected from quantum loop effects, making them attractive as potential steps toward a viable description of quantum gravity [73−75]. One of the most influential formulations in this context is the Deser–Woodard (DW) model [76], originally designed to explain the late-time acceleration of the universe without invoking a finely tuned cosmological constant. Despite its elegant foundation, the first version of the DW model proved to be unsatisfactory on small scales because it lacked an effective screening mechanism that could ensure consistency with observations from the solar system [77]. To overcome this, the same authors developed a revised version [78], which has since been applied successfully in areas such as cosmological evolution [79−83] and the analysis of quasi-normal modes of BHs [84]. The case of exact astrophysical solutions within nonlocal theories remains highly challenging, given the inherent complexity of their equations, often necessitating the use of perturbative or numerical techniques. Static and spherically symmetric spacetimes were also studied under massive infrared modifications of GR in [85], the behavior of linear perturbations in weakly nonlocal quantum-stable theories was tested and shown in [86], and a perturbative Newman–Janis algorithm was used in [87] to investigate slowly rotating BH models in this framework. More recently, a detailed overview of BH-like geometries emerging from nonlocal theories with quadratic curvature terms has been provided in [88], further demonstrating the vitality of this research direction. The revised DW model becomes especially significant, as it not only allows new classes of BH solutions but also shows that, depending on the chosen ansatz for the metric functions, one can either recover the classical Schwarzschild geometry or obtain genuinely novel configurations. When the condition $A(r)=B(r)^{-1}$ is imposed [89], any correction terms vanish under asymptotic flatness, reverting to the Schwarzschild limit. If $A(r)$ is fixed as the Schwarzschild time component while perturbing $B(r)$, regularity requirements enforce a return to GR. However, introducing an inverse power-law correction $A(r)=1-2/r-\alpha/r^n$ [89] leads to the first genuine departures from GR, yielding metrics parametrized by $n>1$ and a small coupling α, which modify key quantities such as the horizon radius, photon sphere, shadow radius, and innermost stable circular orbits (ISCOs) while preserving asymptotic flatness and eliminating unphysical singularities beyond the event horizon. Explicit solutions for $n=2,3,4$ [89] demonstrate finite and well-behaved auxiliary fields, as well as consistent nonlocal distortion functions, with corrections that vanish in the $\alpha\to 0$ limit [89], thereby ensuring compatibility with GR at large scales. In this context, the nonlocal theory of gravity, and in particular its DW refinement, provides a unified scheme in which the familiar Schwarzschild BH arises as a limiting case, while nontrivial deviations emerge in a controlled perturbative regime, marking a concrete step toward embedding BH physics into a broader nonlocal quantum gravity perspective [89].

Quasi-periodic oscillations (QPOs) [90−93] are among the most important observational tools in high-energy astrophysics, appearing as narrow peaks in the X-ray spectra of accreting neutron stars and BH models [94–95]. Their detection across a wide range of frequencies also provides direct access to the physics of accretion flows in regions where relativistic effects are dominant [96–97]. Although low-frequency modes can often be linked to disk precession, magnetic coupling, or global instabilities, high-frequency signals, typically in the hectohertz to kilohertz range, are regarded as direct tracers of orbital and epicyclic motion in curved spacetime [98−105]. Particularly compelling are twin-peak QPOs detected in microquasars such as GRO J1655-40 [106], XTE J1550-564 [107], GRS 1915+105 [108], and H1743-322, where the peaks consistently follow a 3:2 ratio [109]. This strongly supports the idea that they originate from nonlinear resonances between radial and vertical epicyclic frequencies [15], a mechanism naturally allowed by GR due to the splitting of fundamental frequencies at small radii [108, 110–111]. The resonance model not only explains the ratio but also reproduces the observed inverse mass scaling $\nu \propto 1/M$, enabling QPOs to serve as precise diagnostics of the mass and spin of compact objects [112], with fits indicating rapidly rotating BHs with $a \simeq 0.8$–0.96 [113]. Alternative mechanisms such as g-modes, c-modes, or overtone models [114–115] have been proposed but none reproduced the observational patterns as successfully. Similar oscillatory behavior has been identified in neutron stars and even in white dwarfs. However, only BHs exhibit the paired high-frequency resonances, confirming that strong-gravity effects are crucial [116–117]. QPOs provide a rare opportunity to test GR in the strong-field regime and constrain the fundamental parameters of compact objects [118–119]. Upcoming X-ray missions are expected to extend their study to ultraluminous X-ray sources and active galactic nuclei, thus unifying the phenomenology across mass scales [120−122].

QPOs arising from the innermost regions of accretion disks around BHs have been extensively tested in different models [15, 114, 123−128]. Studies of QPOs within braneworld gravity have also been conducted, including several of our previous works [129−132]. The orbital resonance model of QPOs in rotating braneworld Kerr geometries has been discussed in detail [133–134], and ISCOs and test particle motion near charged BHs have been investigated in [135–136]. A comprehensive analysis of the ISCO structure in braneworld scenarios can be found in [137]. The gravitational effects associated with rotating braneworld BHs were analyzed in [138]. On the observational side, X-ray radiation produced by matter accreting close to the horizon provides a crucial tool for testing the strong-field regime of gravity and inferring QPO frequencies. Within GR, these oscillations are often interpreted using relativistic precession models or through the analysis of epicyclic motions. The development of quantum-corrected BH (QC-BH) spacetimes has motivated extensions of such analyses, revealing signatures of quantum corrections that depart from the standard GR predictions. In particular, models incorporating the generalized uncertainty principle show that quantum effects shift the location of ISCOs, leading to modifications in high-frequency QPOs [139−141]. Another important result has been obtained in the framework of loop quantum gravity, where geometric corrections alter the oscillatory spectrum [142−145]. Likewise, noncommutative geometry-based BH models demonstrate that QPO frequencies are strongly influenced by the underlying quantum parameters [146−148]. Systematic studies of QPOs around QC-BHs also provide a promising avenue for testing different approaches to quantum gravity against astrophysical observations, motivating further investigation into their physical origin and observable imprints.

The analysis of test particle motion and associated oscillation frequencies in the present nonlocal BH spacetime is of direct physical relevance, because these quantities constitute invariant diagnostics of the spacetime structure beyond classical GR. The behavior of time-like and null geodesics explicitly reflects how the modified metric functions $h(r)$ and $f(r)$ reshape the effective potential, determine the existence and stability of circular trajectories, and govern the dynamical response to small radial and angular perturbations. Epicyclic frequencies characterize linearized deviations around equilibrium orbits and provide a quantitative measure of strong-field effects induced by the nonlocal parameters α and k, particularly in the vicinity of the horizon. Such frequencies control characteristic timescales of orbital motion, precession, and resonant behavior, and are directly connected to observable phenomena, including quasi-periodic oscillations in accretion flows. A systematic examination of particle dynamics permits a clear separation between genuine nonlocal gravitational modifications and standard relativistic effects while ensuring that the classical Schwarzschild limit is consistently recovered as $\alpha \to 0$. The study of oscillation frequencies and geodesic stability provides a robust framework for assessing the physical implications and phenomenological viability of nonlocal gravity corrections. Our study explores the motion of test particles around static, spherically symmetric BHs within the framework of nonlocal gravity to show the influnece of such modifications to Einstein's theory on the dynamical properties of strong gravitational fields. Although a large number of works already exist in the literature that analyze geodesic structure, orbital stability, and particle collisions within classical GR and various modified gravity theories, the case of nonlocal gravity remains comparatively underexplored despite its growing importance as a promising theoretical framework that addresses ultraviolet divergences, avoids ghost instabilities, and offers a pathway toward reconciling gravitational theory with quantum corrections. The novelty and necessity of our work arise from filling this gap. By examining the geometry and horizons of nonlocal BH solutions and analyzing the corresponding geodesic motion, we provide a systematic account of how nonlocal contributions alter the stability conditions of particle orbits and modify the effective potential governing motion. Special emphasis is placed on ISCOs, which are key observables linked to the efficiency of accretion disks and astrophysical phenomena such as QPOs in X-ray binaries and active galactic nuclei, because their radius and associated dynamical parameters directly influence the energy extraction processes around compact objects. We aim to investigate not only the general influence of these nonlocal BH models but also the explicit role of BH parameters on stability, oscillation frequencies, and energetic processes, clarifying how changes in the underlying geometry leave direct imprints on physical observables. Beyond stable circular orbits, we extend the analysis to perturbed motion and derive the characteristic frequencies of small oscillations, both locally and as observed from infinity, to explicitly show how nonlocal corrections modify precession effects and oscillatory dynamics, which are central to models of QPOs used in interpreting observational data. We further enrich the study by considering high-energy processes through the computation of the center-of-mass energy (CME) of colliding particles near the horizon, demonstrating that nonlocal gravity alters the maximum efficiency of particle acceleration and the energetics of near-horizon collisions, thereby affecting processes related to jet formation and ultra-high-energy emissions. This comprehensive investigation shows that nonlocal gravity produces significant deviations from the predictions of Einstein's GR by reshaping the global structure of BHs, the stability of geodesics, and the energetic efficiency of collisions while providing potential observational signatures that could be tested in astrophysical environments. This study goes beyond existing work by systematically integrating analyses of orbital stability, oscillatory dynamics, and energetic collisions in a nonlocal gravity background, offering both theoretical insights into the nature of strong-field gravity and the practical relevance of connecting modified gravity predictions with astrophysical observations. These justify the importance of the present study despite the abundance of earlier works in the field.

The paper is organized as follows. Section I presents the motivation, theoretical background, and objectives of this study. In Section II, we illustrate BH models, geometries, and horizons in nonlocal gravity, where the metric structure, event horizons, and relevant spacetime properties are discussed in detail. Section III tests particle dynamics around BHs in nonlocal gravity, beginning with the analysis of the effective potential (Section III.A), followed by the characterization of ISCOs (Section III.B), and concluding with the formulation of the effective force governing the motion of the test particles (Section III.C). This study compares the inverse electrodynamics BH with the Schwarzschild BH, emphasizing the effects of additional parameters on particle motion and stability (Section III.D). Section IV is devoted to harmonic oscillations as perturbations of circular orbits, where oscillatory motion is studied through three subsections: frequencies as measured by local observers (Section IV.A), frequencies as observed at infinity (Section IV.B), and the phenomenon of periastron precession (Section. IV.C). Section V analyzes the CME of colliding particles near the BH, illustrating its astrophysical significance. Finally, Section VI presents the conclusions, explains our results, and suggests future work and measurement.

II. BLACK HOLE MODELS, GEOMETRIES, AND HORIZONS IN NONLOCAL GRAVITY

The static, spherically symmetric spacetime corresponding to a nonrotating BH within the framework of nonlocal gravity can be expressed as [89]

$$\mathrm{d}s^2 = -h(r)\,\mathrm{d}t^2 + f(r)\,\mathrm{d}r^2 + \mathrm{d}\mathcal{M}^2_{2\mathcal{D}}, \tag{1}$$

where the radial functions take the form

$$h(r) = 1 - \frac{2}{r} - \frac{\alpha}{r^k}, \tag{2}$$

$$f(r) = 1 - \frac{2}{r} + \left(\frac{\alpha}{3^k (r-3)^2 r^{k+1}}\right)\mathcal{F}, \tag{3}$$

and

$$\mathrm{d}\mathcal{M}^2_{2\mathcal{D}} = r^2\left(\mathrm{d}\theta^2 + \sin^2\theta\,\mathrm{d}\phi^2\right), \tag{4}$$

$$\begin{aligned}\mathcal{F} = {} & 3^k r\,[k(r-3)(r-2) + 4r - 9] \\ & - 3\,[(2r-3)(r-2)]\,r^k.\end{aligned} \tag{5}$$

In these BH models, the dimensionless constant α is assumed to be small ($0 < \alpha \ll 1$) and k is a real parameter greater than unity. The position of the BH horizon is obtained from these conditions $h(r) = 0$ and $f(r) = 0$, which yields

$$r_H = 2 + \frac{\alpha}{2^{k-1}}. \tag{6}$$

The effect of the parameters α and k on the function $h(r)$ is shown in Fig. 1. The value of $h(r)$ increased as α or k increased, illustrating that both parameters contribute positively to the growth of the lapse function.

The static, spherically symmetric spacetime associated with a nonrotating BH in the framework of nonlocal gravity introduces important modifications to the classical Schwarzschild geometry through the radial functions $h(r)$ and $f(r)$, which incorporate corrections controlled by the parameters α and k. The lapse function $h(r)$ contains the standard Schwarzschild term $-2/r$ together with an additional contribution $-\alpha/r^k$, and the radial component $f(r)$ carries a more intricate correction involving the function $\mathcal{F}$, which reflects the nonlocal character of the theory. The parameter α, assumed to be small and positive ($0<\alpha\ll 1$), determines the general strength of these deviations, and the exponent $k>1$ dictates the fall-off behavior of the correction with radial distance. In the limit $\alpha\to 0$, one naturally recovers the Schwarzschild BH, confirming that the nonlocal model smoothly reduced to general relativity in the absence of the new interaction. For large r, the influence of the corrections fades away because the additional terms scale as inverse powers of r. The position of the event horizon, determined by solving $h(r)=0$ or $f(r)=0$, slightly shifted from the classical value $r=2$ to $r_H=2+\alpha/2^{k-1}$, indicating that the radius of the horizon expands with increasing α, and the influence of k appears as a modulation factor in this displacement. The analysis of the lapse function shows that both α and k act to increase its magnitude, which can be interpreted as a weakening of the gravitational redshift relative to the Schwarzschild case. For small values of k (just above unity), the correction term decays slowly with r, making the nonlocal effect more significant at larger distances, whereas higher k leads to faster decay and more localized deviations near the horizon. Thus, the combined influence of α and k provides a tunable modification to the classical geometry: α controls the amplitude of the deviation, and k governs its radial profile. This nonlocal BH metric reveals how small corrections can alter the near-horizon structure, shift the location of the event horizon, and influence the redshift behavior while preserving the classical Schwarzschild form as a limiting case.

III. PARTICLE DYNAMICS AROUND BH IN NONLOCAL GRAVITY

The motion of a neutral particle is described by the Hamiltonian [149−159]:

$$H=\frac{1}{2}g^{\zeta\eta}p_\zeta p_\eta+\frac{1}{2}\mu^2, \tag{7}$$

where μ stands for the particle mass.

The relation $p^\zeta=\mu u^\zeta$ gives the four-momentum, with $u^\zeta=\mathrm{d}x^\zeta/\mathrm{d}\tau$ being the four-velocity and τ the proper time. From this Hamiltonian, the equations of motion follow [149−160]:

$$\frac{\mathrm{d}x^\eta}{\mathrm{d}\zeta}\equiv\mu u^\eta=\frac{\partial H}{\partial p_\eta},\quad \frac{\mathrm{d}p_\eta}{\mathrm{d}\zeta}=-\frac{\partial H}{\partial x^\eta}, \tag{8}$$

where $\zeta=\tau/\mu$ illustrates the role of the affine parameter. Owing to BH symmetry, two conserved quantities appear: the particle's specific energy E and angular momentum L, expressed as

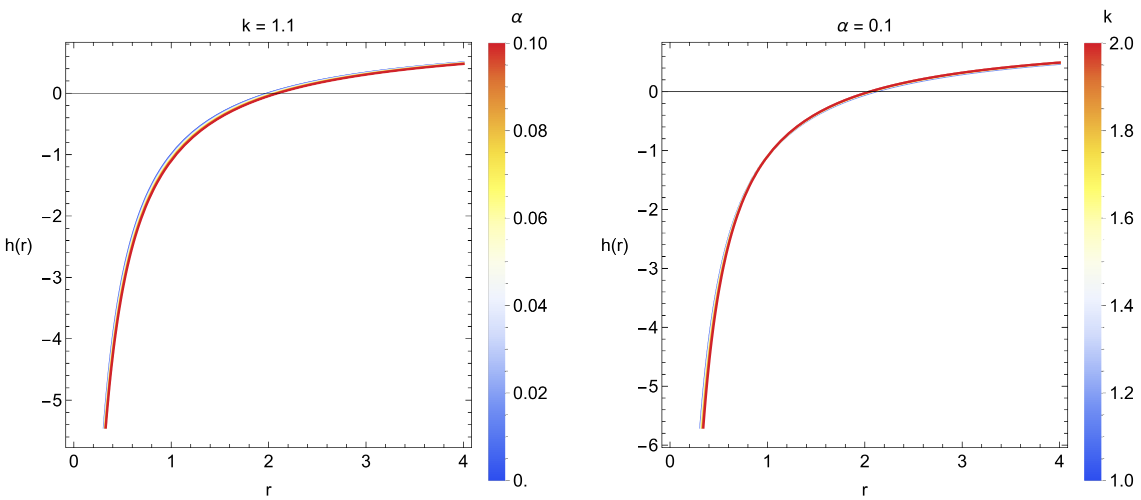

Fig. 1. (color online) Radial behavior of the lapse function $h(r)$ for a static, spherically symmetric BH in nonlocal gravity. **(i) Left panel:** $h(r)$ versus the radial coordinate r for fixed $(k=1.1)$ and varying nonlocal parameter $(\alpha=0,0.02,0.04,0.06,0.08,0.10)$. **(ii) Right panel:** $h(r)$ for fixed $(\alpha=0.1)$ and different values of $(k=1.0,1.2,1.4,1.6,1.8,2.0)$. Increasing (α) or k enhances the metric function and shifts the event horizon outward relative to the Schwarzschild case.

$$\frac{p_t}{m} = -\frac{\alpha}{r^k} - \frac{2}{r} + 1, \tag{9}$$

$$\frac{p_\phi}{m} = r^2 \sin^2\theta \frac{\mathrm{d}\phi}{\mathrm{d}\tau} = \mathcal{L}, \tag{10}$$

where $\mathcal{E} = E/m$ and $\mathcal{L} = L/m$ denote the particle's energy and angular momentum per unit mass, respectively. The corresponding equations that govern motion determine the temporal u^t, angular u^ϕ, and radial u^r components of the four-velocity u^α.

$$\dot{t} = \frac{\mathcal{E}}{\left(-\frac{\alpha}{r^k} - \frac{2}{r} + 1\right)}, \tag{11}$$

$$\dot{\phi} = \frac{\mathcal{L}}{r^2 \sin^2\theta}, \tag{12}$$

$$\dot{r}^2 + \left(\epsilon + \frac{\mathcal{L}^2}{r^2 \sin^2\theta}\right)\left(-\frac{\alpha}{r^k} - \frac{2}{r} + 1\right) = \mathcal{E}^2, \tag{13}$$

where $\epsilon = 1$ corresponds to time-like particles and $\epsilon = 0$ to light-like particles. The dot indicates differentiation with respect to τ. Using the normalization condition $p^\alpha p_\alpha = -1$, the effective potential takes the form

$$V_{\rm eff}(r,\theta) = \left(1 + \frac{\mathcal{L}^2}{r^2}\csc^2\theta\right)\left(1 - \frac{2}{r} - \frac{\alpha}{r^k}\right). \tag{14}$$

Hence, the angular term $\mathcal{L}^2/\left(r^2\sin^2\theta\right)$ can be equivalently written as $\mathcal{L}^2\csc^2\theta/r^2$, which preserves the mathematical form of the effective potential while making explicit the centrifugal divergence near $\theta \to (0,\pi)$.

$$V_{\rm eff}(r,\theta) = \left(1 + \frac{\mathcal{L}^2}{r^2\sin^2(\theta)}\right)\left(-\frac{\alpha}{r^k} - \frac{2}{r} + 1\right). \tag{15}$$

• Case of $\alpha \to 0$:

In this limit, the results illustrate the Schwarzschild BH models ($M = 1$)

$$V_{\rm eff}(r,\theta) = \left(1 + \frac{\mathcal{L}^2}{r^2\sin^2(\theta)}\right)\left(-\frac{2}{r} + 1\right). \tag{16}$$

A. Effective potential in nonlocal gravity

The concept of effective potential $V_{\rm eff}(r,\theta)$ plays a central role in examining the dynamics of the test particles because it provides a way to illustrate their motion without the need to directly integrate the entire set of equations of motion. The $V_{\rm eff}$ parameters illustrate the location of unstable and stable circular orbits. In Fig. (2), we show how the effective potential changes with the radial distance r. The minima of the curves correspond to stable circular orbits, while the maxima identify the positions of unstable ones. The first column of the figure illustrates the variation of $V_{\rm eff}$ for different choices of the BH parameter k, while the second column demonstrates the effect of the BH parameter α. As k or α increases, the minima of the effective potential move closer to the BH horizon, and the overall magnitude of $V_{\rm eff}$ increase. For circular equatorial orbits, the following requirements must be satisfied [149−160]:

$$V_{\rm eff}(r) = \mathcal{E}^2, \quad \frac{\mathrm{d}V_{\rm eff}(r)}{\mathrm{d}r} = 0. \tag{17}$$

Solving Eq. (17) leads to the expression for circular orbits in the geometry of a BH in nonlocal gravity, yielding the angular momentum

$$\mathcal{L} = \frac{r\sqrt{\alpha k r^{-k} + \frac{2}{r}}}{\sqrt{-\left(\alpha(k+2)r^{-k}\right) - \frac{6}{r} + 2}}, \tag{18}$$

together with the corresponding specific energy

$$\mathcal{E} = \frac{r^{-k-1}\left(r^{k+1} - 2r^k - \alpha r\right)}{\sqrt{-\frac{1}{2}\alpha(k+2)r^{-k} - \frac{3}{r} + 1}}. \tag{19}$$

• Figure 3 illustrates how the angular momentum $\mathcal{L}$ behaves for equatorial circular orbits around a nonrotating BH in the framework of nonlocal gravity. Figure 3 clearly shows that $\mathcal{L}$ increases as the BH parameter α increases. When the BH parameter k takes higher values, the angular momentum becomes smaller. The figure also shows that $\mathcal{L}$ increases steadily as the radial distance r increases.

• Figure 4 presents the variation of the energy $\mathcal{E}$ corresponding to circular equatorial orbits in the same background. The plot indicates that for circular orbits, the energy initially increases when the BH parameter α increases; however, after a certain stage it starts to decline for larger α. A comparable trend is observed when the parameter is changed to k. The figure also shows that the energy $\mathcal{E}$ of the particles increases as the orbital radius r increases.

B. ISCOs in nonlocal gravity

The positions of stable and unstable circular trajectories are identified through the minimum and maximum of the effective potential, respectively. In the framework of

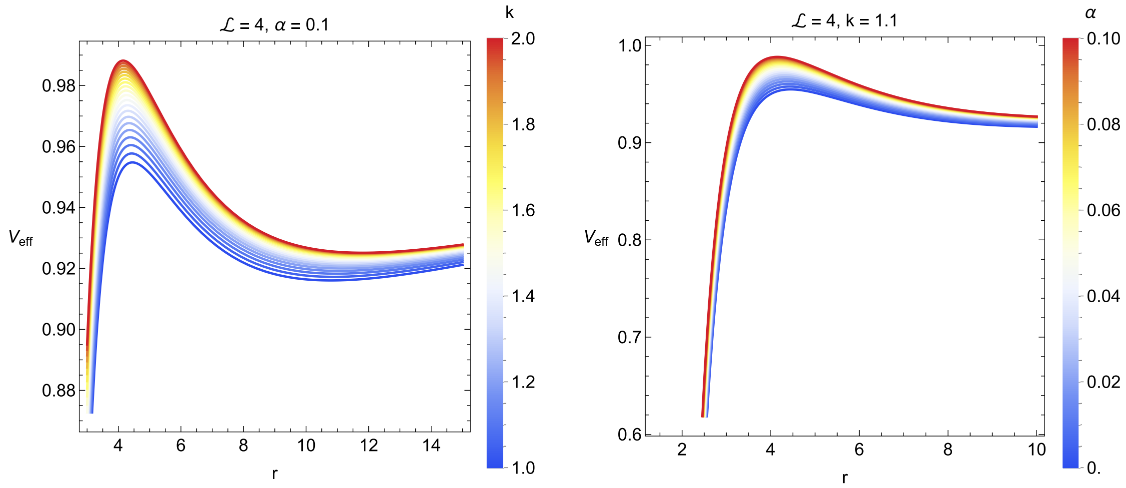

Fig. 2. (color online) Effective potential $V_{\rm eff}(r)$ of neutral test particles moving in the equatorial plane of a nonrotating BH in nonlocal gravity. The angular momentum is fixed at $\mathcal{L}=4$. **(i) Left panel:** Variation of $V_{\rm eff}$ with r for fixed $\alpha=0.1$ and different values of $k=1.0,1.2,1.4,1.6,1.8,2.0$. **(ii) Right panel:** $V_{\rm eff}$ for fixed $k=1.1$ and varying $\alpha=0,0.02,0.04,0.06,0.08,0.10$. The minima and maxima correspond to stable and unstable circular orbits, respectively.

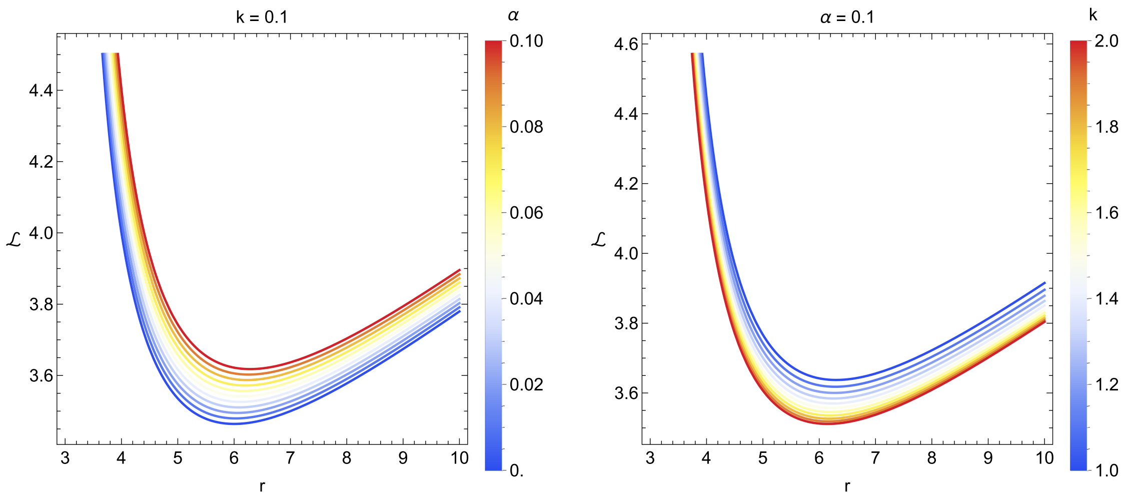

Fig. 3. (color online) Angular momentum $\mathcal{L}$ of equatorial circular orbits as a function of the radial coordinate r in nonlocal gravity. **(i) Left panel:** $\mathcal{L}(r)$ for fixed $k=1.1$ and varying $\alpha=0,0.02,0.04,0.06,0.08,0.10$. **(ii) Right panel:** $\mathcal{L}(r)$ for fixed $\alpha=0.1$ and different values of $k=1.0,1.2,1.4,1.6,1.8,2.0$. The angular momentum increases with r and α, and decreases as k increases.

Newtonian mechanics, the effective potential always develops a minimum for any given angular momentum and an ISCO does not exist. The situation becomes different when the potential explicitly depends both on the angular momentum of the particle and additional parameters. Within GR, for instance, test particles moving near a Schwarzschild BH experience an effective potential that generally has two turning points for each angular momentum. When these two extrema merge into one, the ISCO is formed, located at $r=3r_g$, with r_g being the Schwarzschild radius. To determine the ISCO, the following conditions are imposed [149−160].

$$V_{\rm eff}(r)=\mathcal{E}^2, \qquad \frac{{\rm d}V_{\rm eff}(r)}{{\rm d}r}=0, \qquad \frac{{\rm d}^2V_{\rm eff}(r)}{{\rm d}r^2}=0. \tag{20}$$

For a nonrotating BH influenced by non-local gravity, the ISCOs radii are given by

$$\frac{r^{-k-1}\left(2\alpha\left(k^2-6k-1\right)r^{k+1}-\alpha(k-2)kr^{k+2}-12r^{2k}+2r^{2k+1}-\alpha^2k(k+2)r^2\right)}{\left(2r^{k+1}-6r^k-\alpha(k+2)r\right)\sqrt{\alpha kr^{-k}+\dfrac{2}{r}}\sqrt{-\left(\alpha(k+2)r^{-k}\right)-\dfrac{6}{r}+2}}=0, \tag{21}$$

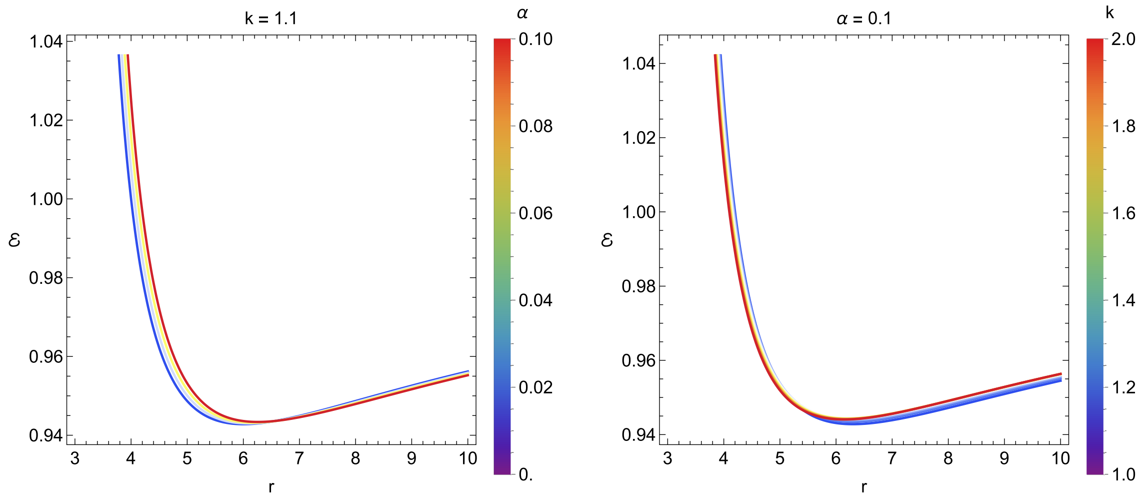

Fig. 4. (color online) Specific energy $\mathcal{E}$ of neutral test particles on equatorial circular orbits in the nonlocal gravity BH spacetime. **(i) Left panel:** $\mathcal{E}(r)$ for fixed $k=1.1$ and varying $\alpha=0, 0.02, 0.04, 0.06, 0.08, 0.10$. **(ii) Right panel:** $\mathcal{E}(r)$ for fixed $\alpha=0.1$ and different values of $k=1.0, 1.2, 1.4, 1.6, 1.8, 2.0$. The energy increases with radial distance and shows a nonmonotonic dependence on nonlocal parameters.

● Figure 5 shows the equatorial ISCOs around a static BH in nonlocal gravity. The left panel illustrates the dependence of ISCOs on the BH parameter α, and the right panel demonstrates their variation with the parameter k. The ISCO radius increases with higher values of α, and decreases as k becomes stronger.

The exact equations for the angular momentum and specific energy are obtained directly from the condition for circular orbits of the effective potential.

$$V'_{\text{eff}}(r) = 0. \tag{22}$$

This condition corresponds to the vanishing of the radial force, which provides the necessary criterion for a stable circular orbit in the BH spacetime considered. The algebraic complexity observed in these expressions originates from nonlocal gravity corrections, which introduce additional terms proportional to r^{-k}. These terms modify the standard general relativistic behavior and are responsible for the more intricate functional form of the angular momentum and energy.

To determine the ISCOs, we simultaneously impose

$$V'_{\text{eff}}(r_{\text{ISCO}}) = 0, \quad V''_{\text{eff}}(r_{\text{ISCO}}) = 0, \tag{23}$$

which identifies the minimal radius at which a stable circular orbit can exist. Although the derivatives involved are algebraically extensive, they are fully compatible with the expressions for angular momentum and energy, demonstrating how these quantities satisfy the ISCO conditions. This provides complete algebraic transparency and verifies that the results are consistent within the framework of nonlocal gravity.

C. Effective force in nonlocal gravity

The effective force on a test particle describes the nature of its motion, that is, whether the trajectory is drawn inward toward the BH or pushed outward. In the background of a static BH governed by nonlocal gravity, the dynamics allow for both attractive and repulsive gravitational interactions. Using Eq. (17), the effective force can be expressed as [149–160]

$$\begin{aligned} F &= -\frac{1}{2}\frac{\mathrm{dV}_{\text{eff}}}{\mathrm{d}r}, \\ &= \frac{1}{2} r^{-k-4}\left(\mathcal{L}^2\left(2r^{k+1} - 6r^k - \alpha(k+2)r\right)\right. \\ &\quad \left. - r^2\left(2r^k + \alpha k r\right)\right). \end{aligned} \tag{24}$$

● Figure 6 shows the variations of the effective force with the radial coordinate r for different choices of the BH parameters α and k. The left column shows how the force changes with α, and the right column corresponds to the changes with k. The influence shows that increasing α strengthens the attractive nature of the force, while increasing k leads to a repulsive effect.

D. Comparison with the Schwarzschild black hole model

To illustrate the impact of nonlocal gravity corrections on the particle dynamics, the obtained results must be compared with those of the classical Schwarzschild BH model, which can be recovered from the present model by setting $\alpha \to 0$ and $k \to 1$. The metric function simplifies to the well-known form

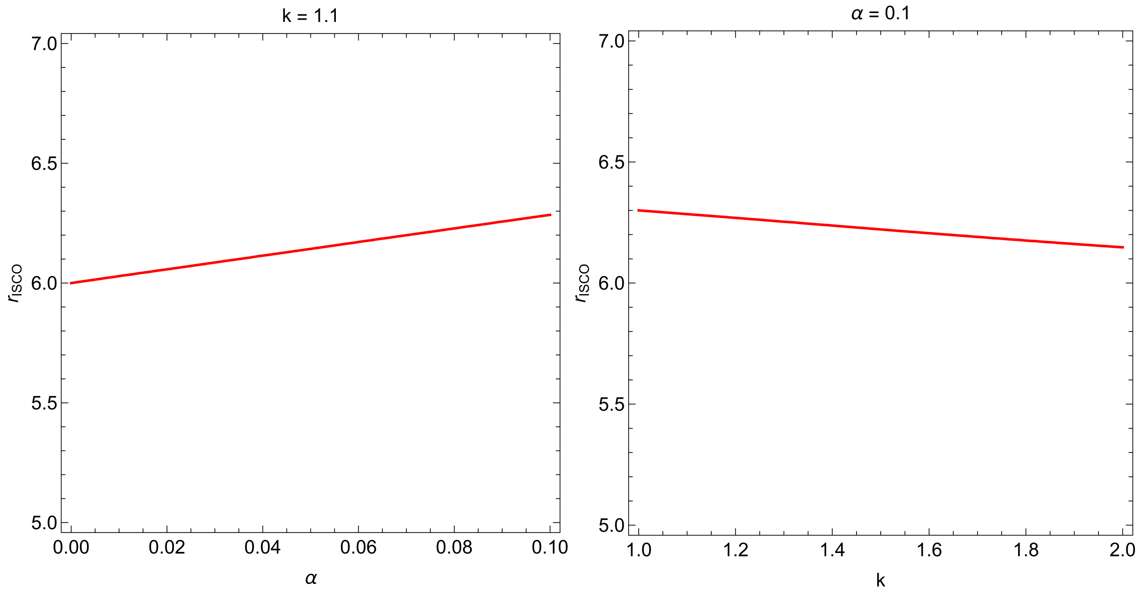

Fig. 5. (color online) Dependence of the ISCO radius $r_{\rm ISCO}$ on the nonlocal gravity parameters. **(i) Left panel:** $r_{\rm ISCO}$ as a function of α for fixed $k=1.1$. **(ii) Right panel:** $r_{\rm ISCO}$ as a function of k for fixed $\alpha=0.1$. The ISCO radius increases with α and decreases as k increases, deviating from the Schwarzschild value $r_{\rm ISCO}=6$.

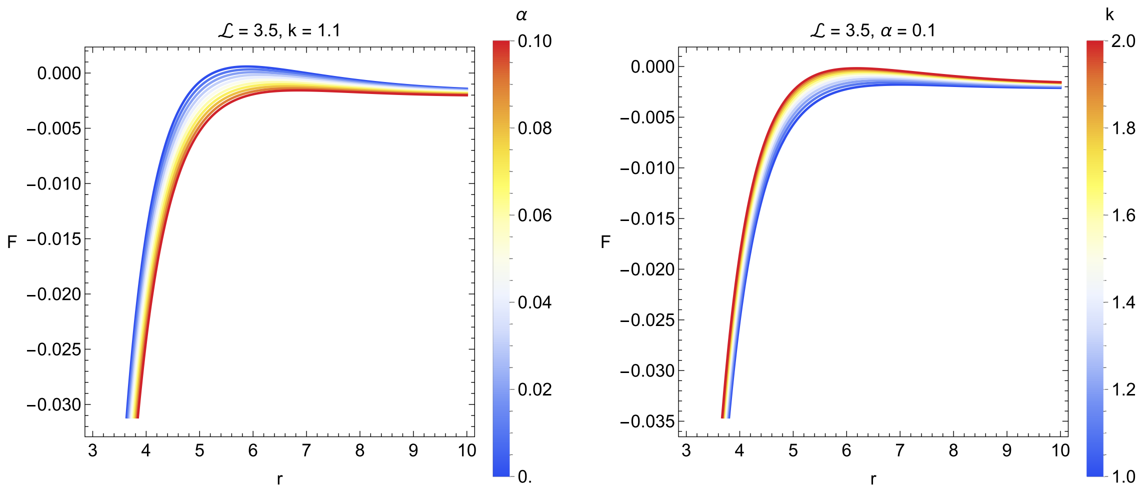

Fig. 6. (color online) Radial profile of the effective force F acting on neutral test particles orbiting a nonrotating BH in nonlocal gravity. The angular momentum is fixed at $\mathcal{L}=3.5$. **(i) Left panel:** Effective force for fixed $k=1.1$ and varying $\alpha=0,0.02,0.04,0.06,0.08,0.10$. **(ii) Right panel:** Effective force for fixed $\alpha=0.1$ and different values of $k=1.0,1.2,1.4,1.6,1.8,2.0$. Increasing α strengthens the attractive force, while larger k introduces repulsive features.

$$f(r)=1-\frac{2}{r}, \tag{25}$$

and the corresponding effective potential reduces to

$$V_{\rm eff}^{\rm Sch}(r,\theta)=\left(1+\frac{\mathcal{L}^2}{r^2\sin^2\theta}\right)\left(1-\frac{2}{r}\right). \tag{26}$$

This expression serves as the information for testing the influence of the parameters (α,k) that encode the nonlocal gravitational corrections.

1. *Measurement of effective potential*

In the study of the influence of the nonlocal gravity BH model, the effective potential $V_{\rm eff}(r,\theta)$ is defined with additional terms illustrated by α and k parameters, which test the influence of BH properties. Increasing α deepens the potential parameters, showing a stronger gravitational attraction near the event horizon, and larger values of k shift the minima closer to the horizon. The Schwarzschild BH model illustrate a single minimum that corresponds to the location of the stable circular orbit. The presence of (α,k) introduces additional degrees of freedom that can either strengthen or weaken the gravitational confinement depending on their magnitudes.

2. *Measurement of angular momentum and energy of circular orbits properties*

In the case of circular trajectories, the specific energy $\mathcal{E}$ and angular momentum $\mathcal{L}$ indicate the modifications shown by the BH model. When $\alpha > 0$, the angular momentum required to maintain circular motion increases relative to the Schwarzschild case, and higher k values lead to a reduction in $\mathcal{L}$. The energy profile exhibits a more complex behavior: $\mathcal{E}$ initially increases with α, then slightly decreases for large values of α. In the Schwarzschild background, $\mathcal{E}$ and $\mathcal{L}$ vary monotonically with the orbital radius, and the relations between them remain uniquely determined by the metric function model $f(r) = 1 - 2/r$. The nonlocal contributions modify the balance between centrifugal and gravitational forces, leading to different orbital energy requirements.

3. *ISCO comparison*

The measurment of ISCO results show another distinction between the two geometries. For the Schwarzschild BH, the ISCO radius is located at $r_{\rm ISCOs} = 6M = 6$, corresponding to the merging of the stable and unstable points of $V_{\rm eff}$. However, in the nonlocal gravity scenario, this location depends on (α, k). An increase in α tends to push the ISCO outward, implying that stable circular motion is possible only farther from the BH, while an increase in k produces the opposite effect, reducing $r_{\rm ISCOs}$. Thus, the parameters of nonlocality directly control the extent of the stable orbital region.

4. *Effective force*

The effective force derived from this relation $F = -\dfrac{1}{2}\dfrac{{\rm d}V_{\rm eff}}{{\rm d}r}$ reveals that in the Schwarzschild case, the interaction is purely attractive and decays monotonically as r increases. However, in the framework of nonlocal gravity, the behavior of $F(r)$ becomes richer: for small r, the force remains attractive; however, depending on (α, k), it can exhibit a partial repulsive phase near the horizon. Increasing α strengthens the inward pull, and higher k values can introduce a repulsive contribution at intermediate distances. These deviations suggest that the effective curvature corrections of nonlocal gravity alter the local spacetime geometry and nature of the gravitational field around the compact object.

The Schwarzschild BH model serves as the limiting configuration of the present model, and nonlocal gravity introduces two tunable parameters (α, k) that modify the intensity and structure of the gravitational potential. The main differences can be illustrated as follows:

- $V_{\rm eff}$ in nonlocal gravity shows deeper or shifted minima compared to the Schwarzschild potential.

- $\mathcal{L}$ increases with α but decreases with k, and $\mathcal{E}$ shows nonmonotonic dependence on α.

- The ISCO radius increases with α and decreases with k, deviating from the fixed Schwarzschild value $r_{\rm ISCO} = 6$.

- The effective force F may exhibit repulsive features, unlike the purely attractive Schwarzschild case.

Another important result is that the Schwarzschild spacetime appears as a special and less flexible case of the more general nonlocal gravity framework in which the additional parameters offer a mechanism to fine-tune particle motion and orbital stability around BHs.

IV. HARMONIC OSCILLATIONS AS PERTURBATIONS OF CIRCULAR ORBITS IN NONLOCAL GRAVITY BLACK HOLE MODELS

To explore the oscillatory motion of neutral particles, we slightly disturb the equations of motion around stable circular paths. When a test particle is shifted slightly from its equilibrium point in the equatorial plane condition, it follows an epicyclic path, which can be described as linear harmonic oscillations [149−160].

A. Frequency measurements by local observer in nonlocal gravity black hole models

The frequencies of these harmonic oscillations, as measured by a local observer, are expressed as [149−160]

$$\omega_r^2 = \frac{-1}{2}\frac{\partial^2 V_{\rm eff}(r,\theta)}{\partial r^2}, \tag{27}$$

$$\omega_\theta^2 = \frac{1}{2}\frac{g_{rr}(r,\theta)}{r^2}\frac{\partial^2 V_{\rm eff}(r,\theta)}{\partial \theta^2}, \tag{28}$$

$$\omega_\phi = \frac{{\rm d}\phi}{{\rm d}\tau}. \tag{29}$$

where ω_r, ω_θ, and ω_ϕ represent the radial, vertical, and orbital (axial) frequencies of a neutral test particle moving around in the nonlocal gravity BH model, respectively. They take the following explicit forms:

$$\omega_r^2 = \frac{1}{2}r^{-k-5}\big(\mathcal{L}^2(\alpha\left(k^2+5k+6\right)r - 6r^{k+1} + 24r^k) + r^2\left(4r^k + \alpha k(k+1)r\right)\big), \tag{30}$$

$$\omega_\theta^2 = \frac{2r^k + \alpha kr}{r^2\left(2r^{k+1} - 6r^k - \alpha(k+2)r\right)}, \tag{31}$$

$$\omega_\phi^2 = \frac{2r^k + \alpha kr}{r^2\left(2r^{k+1} - 6r^k - \alpha(k+2)r\right)}. \tag{32}$$

B. Frequency measurement properties in the case of a distant observer in nonlocal gravity BH models

The locally defined angular frequencies ω_β are introduced in Eqs. (30)–(32). The angular frequencies recorded by a static observer far away, denoted as Ω, are expressed as [149–160]

$$\Omega_\beta = \omega_\beta \frac{d\tau}{dt}, \tag{33}$$

where the factor $d\tau/dt$ represents the redshift correction, given by

$$\frac{dt}{d\tau} = -\frac{\mathcal{E}}{g_{tt}}. \tag{34}$$

When the frequencies of small oscillations are described in physical units as observed from infinity, the corresponding frequencies for neutral particles are given by [149–159]

$$\nu_i = \frac{1}{2\pi}\frac{c^3}{GM}\Omega_i, \tag{35}$$

where ν_i represents the physical frequencies measured by a distant observer (Hz), and the index $i \in r,\theta,\phi$ labels the radial, polar, and azimuthal components, respectively. Here, Ω_r, Ω_θ, and Ω_ϕ denote the dimensionless radial, polar, and azimuthal frequencies measured at infinity, respectively, given by

$$\Omega_r^2 = -\frac{1}{\chi(r,\alpha,k)}[3^k(r-3)^2(-2\alpha\left(k^2-6k-1\right)r^{k+1} + \alpha(k-2)kr^{k+2} + 12r^{2k} - 2r^{2k+1} + \alpha^2 k(k+2)r^2)], \tag{36}$$

$$\Omega_\theta^2 = \frac{1}{2}\alpha kr^{-k-2} + \frac{1}{r^3}, \tag{37}$$

$$\Omega_\phi^2 = \frac{1}{2}\alpha kr^{-k-2} + \frac{1}{r^3}, \tag{38}$$

where

$$\begin{aligned}\chi(r,\alpha,k) = {} & 2r^2\left(r^{k+1} - 2r^k - \alpha r\right)(21\left(\alpha + 3^k\right)r^{k+1} \\ & - 2\left(3\alpha + 4\,3^k\right)r^{k+2} + 3^k r^{k+3} \\ & - 18\left(\alpha + 3^k\right)r^k + \alpha 3^k kr^3 - \alpha 3^k(5k-4)r^2 \\ & + \alpha 3^{k+1}(2k-3)r).\end{aligned} \tag{39}$$

• Figure 7 illustrates the behavior of the radial variation of the oscillation frequencies ν_j for neutral particles near a static BH in nonlocal gravity. The orbital frequency Ω_ϕ coincides with the polar frequency Ω_θ. The first panel (top-left) corresponds to the usual Schwarzschild case. The increase in the BH parameter α is shown to shift the radial frequency curves outward, moving them further from the horizon. Larger values of the parameter k push the frequency profiles inward, closer to the event horizon.

C. Testing periastron precession in black hole spacetimes of nonlocal gravity

We look at the periastron frequency of a neutral test particle moving around a nonrotating BH in nonlocal gravity. The study is conducted by considering small disturbances near the equatorial plane at $\pi/2$. To evaluate the periastron precession, we slightly shift the particle from its stable orbit, which produces oscillations about that point with radial frequency Ω_r. The periastron frequency, written as Ω_P, is then obtained as the difference between the orbital frequency Ω_ϕ and radial frequency Ω_r given by [149–160]

$$\Omega_P = \Omega_\phi - \Omega_r. \tag{40}$$

Figure 8 illustrates the behavior of the periastron frequency in the background of such a BH. The first panel displays the variation of Ω_P with different values of the parameter α. The second panel presents the case for different values of k. The increase in k reduces the frequency of the periastron, while the larger values of α improve it. Ω_P also decreases as the radial distance r increases.

V. INFLUENCE OF CME PROPERTIES IN NONLOCAL BLACK HOLE MODELS

In this section, we study the collision of two neutral test particles, each having the same rest mass μ but moving with different four-velocities while lying on the same plane. The CME for this system is expressed as [149–160]

$$\frac{E_{\rm cm}}{\sqrt{2}m_0} = \sqrt{1 - g_{\alpha\beta}u^\alpha u^\beta}, \tag{41}$$

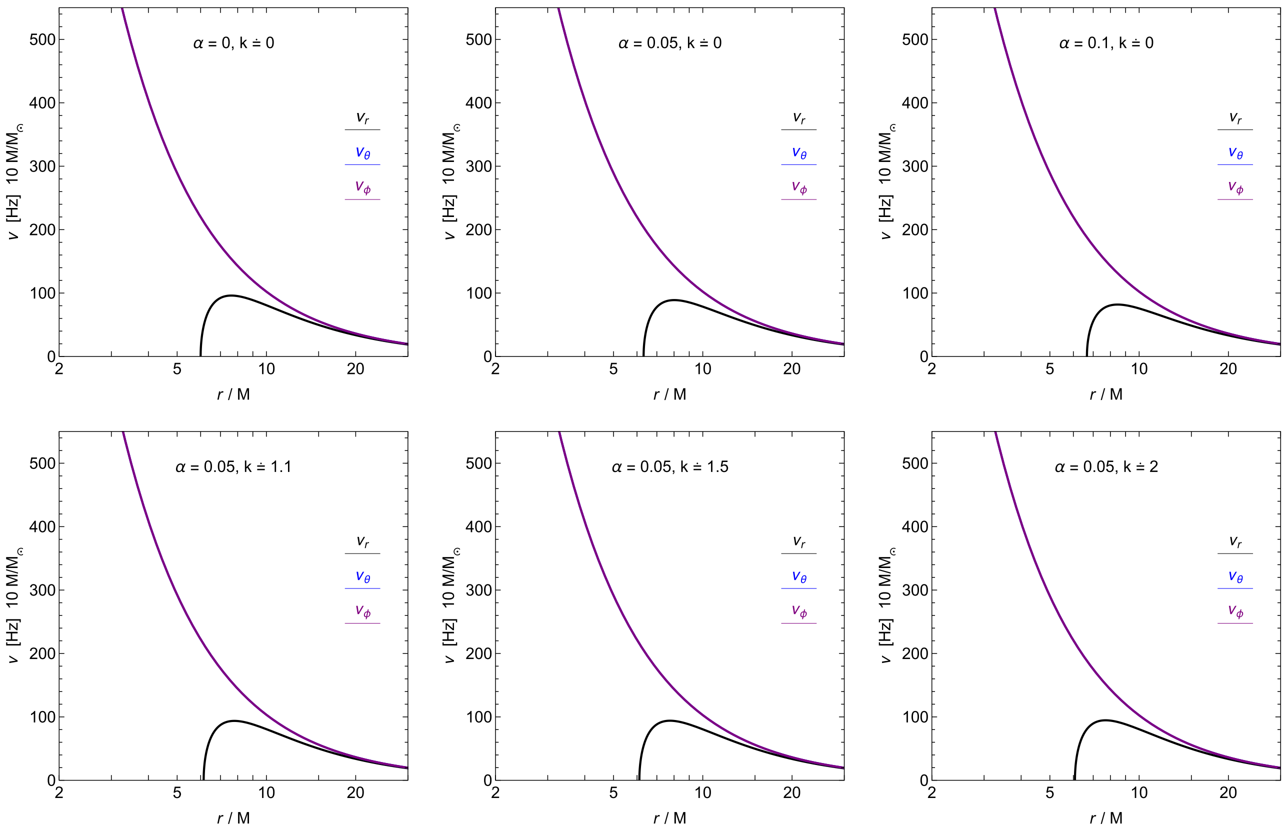

Fig. 7. (color online) Radial, vertical, and orbital frequencies $(\nu_r, \nu_\theta, \nu_\phi)$ of neutral test particles measured by a distant observer for a BH of mass $M = 10, M_\odot$ in nonlocal gravity. The frequencies are shown as functions of the radial coordinate r/M. **(i) Top left panel:** Schwarzschild limit ($\alpha = 0$). **(ii) Top right and middle panels:** Fixed k with increasing values of α. **(iii) Bottom panels:** Fixed $\alpha = 0.05$ and varying $k = 1.1, 1.5, 2.0$. The orbital and vertical frequencies coincide, while the radial frequency is strongly affected by the nonlocal parameters.

where

$$u_i^\alpha = \left(\frac{\mathcal{E}_i}{\left(-\dfrac{\alpha}{r^k} - \dfrac{2}{r} + 1\right)}, -Y_i, 0, \frac{\mathcal{L}_i}{r^2} \right), \tag{42}$$

and

$$Y_i = \sqrt{\mathcal{E}_i^2 - \left(1 + \frac{\mathcal{L}^2}{r^2}\right)\left(-\frac{\alpha}{r^k} - \frac{2}{r} + 1\right)}, \quad i = 1, 2. \tag{43}$$

where $\mathcal{E}_i$ and $\mathcal{L}_i$ denote the conserved energy and angular momentum of each particle, respectively. The value of the CME depends both on the motion of the particles and the background gravitational field near the compact object. For two colliding particles, it combines their rest masses with their kinetic contributions. In the case of a static, nonrotating BH in nonlocal gravity, it takes the form

$$\frac{E_{\rm cm}}{\sqrt{2} m_0} = \sqrt{1 + \frac{\mathcal{E}_1 \mathcal{E}_2}{h(r)} - \frac{Y_1 Y_2}{h(r)} - \frac{\mathcal{L}_1 \mathcal{L}_2}{r^2}}, \tag{44}$$

In this case, we can write this equation

$$\frac{E_{\rm cm}}{\sqrt{2} m_0} = \sqrt{\frac{\mathcal{E}_1 \mathcal{E}_2 - \zeta_1 \zeta_2}{-\alpha r^{-k} - \dfrac{2}{r} + 1} - \frac{\mathcal{L}_1 \mathcal{L}_2}{r^2} + 1}, \tag{45}$$

where the functions ζ_1 and ζ_2 are given by

$$\zeta_1 = \sqrt{\mathcal{E}_1^2 - \left(\frac{\mathcal{L}_1^2}{r^2} + 1\right)\left(-\alpha r^{-k} - \frac{2}{r} + 1\right)}. \tag{46}$$

and

$$\zeta_2 = \sqrt{\mathcal{E}_2^2 - \left(\frac{\mathcal{L}_2^2}{r^2} + 1\right)\left(-\alpha r^{-k} - \frac{2}{r} + 1\right)}. \tag{47}$$

• Figure 9 shows the behavior of the CME with the radial distance r for a nonrotating BH in nonlocal gravity.

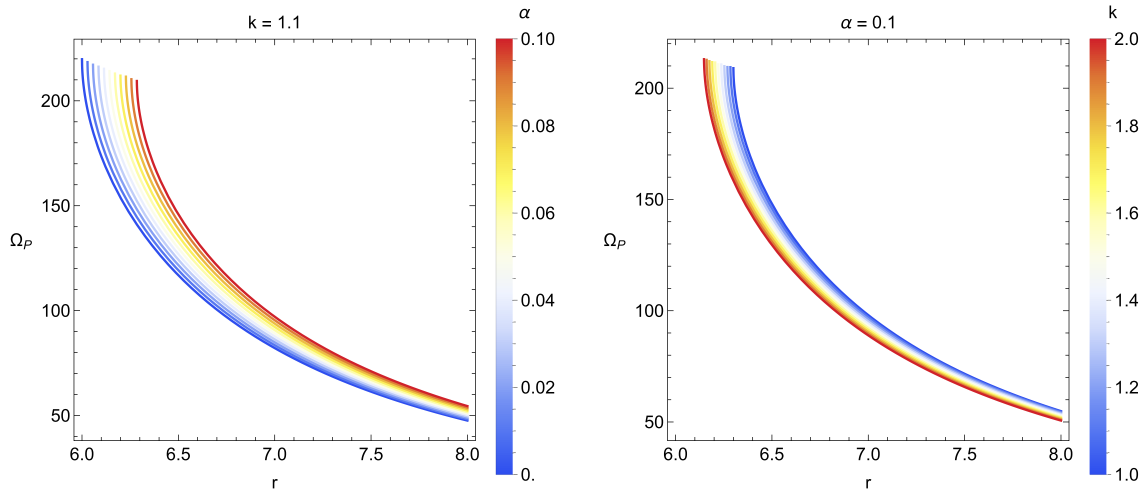

Fig. 8. (color online) Periastron precession frequency Ω_P for neutral test particles orbiting a nonrotating BH in nonlocal gravity. **(i) Left panel:** Ω_P as a function of r for fixed $k = 1.1$ and varying $\alpha = 0, 0.02, 0.04, 0.06, 0.08, 0.10$. **(ii) Right panel:** Ω_P for fixed $\alpha = 0.1$ and different values of $k = 1.0, 1.2, 1.4, 1.6, 1.8, 2.0$. The periastron frequency increases with α and decreases as k increases.

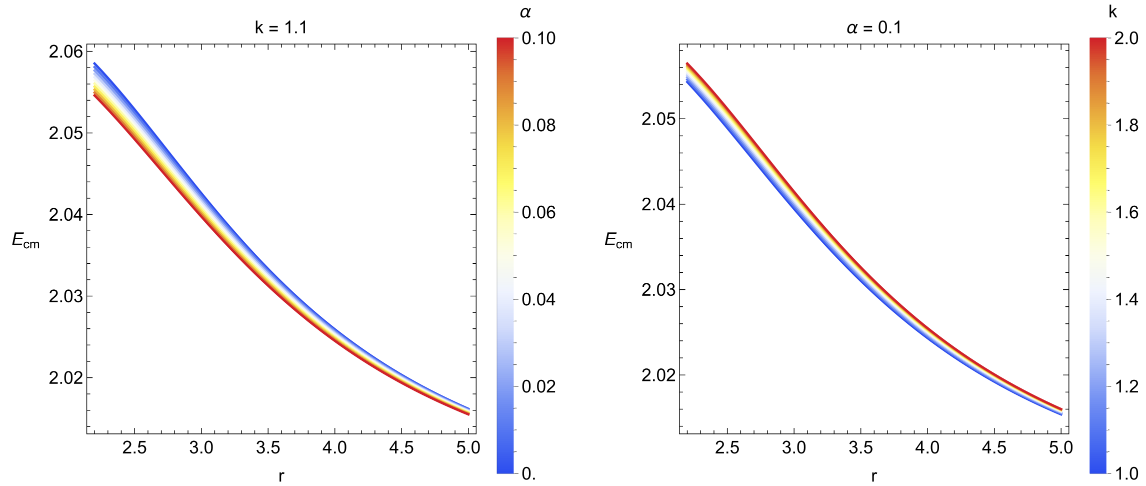

Fig. 9. (color online) Center-of-mass energy (CME) of two neutral particles colliding near a nonrotating BH in nonlocal gravity as a function of the radial coordinate r. **(i) Left panel:** CME for fixed $k = 1.1$ and varying $\alpha = 0, 0.02, 0.04, 0.06, 0.08, 0.10$. **(ii) Right panel:** CME for fixed $\alpha = 0.1$ and different values of $k = 1.0, 1.2, 1.4, 1.6, 1.8, 2.0$. The CME increases near the horizon is enhanced by larger k, and suppressed by increasing α.

Collisions near the horizon can be seen to generate large energies. Increasing the parameter k raises the CME, and larger values of α reduce it. As the distance r increases, the radial profile of the CME decreases steadily.

Although several recent studies have explored the dynamics of test particles and QPOs in modified theories of gravity, the present work illustrates the formulation and physical interpretation of nonlocal corrections to BH spacetimes. Unlike earlier approaches that either treated nonlocal effects perturbatively or confined the analysis to qualitative estimates, this study provides a systematic and self-consistent analytical treatment of geodesic motion, orbital stability, harmonic oscillations, and energy extraction processes around static, spherically symmetric nonlocal BHs characterized by the parameters (α, k). The novelty lies in simultaneously integrating these diverse dynamical aspects (showing the influence of BH parameters on particle dynamics measurement), effective potential, ISCOs, epicyclic frequencies, and CMEs of particle collisions within a single coherent framework of nonlocal gravity, allowing for a direct comparative analysis with the classical Schwarzschild BH model limit. The physical implications of nonlocal parameters are also thoroughly tested, showing how small deviations from Einstein's theory can lead to measurable differences in orbital frequencies and energetic processes near the event horizon. These analytical derivations of frequency shifts and force profiles distinguish the present work from previous investigations that often focused on isolated aspects such as ISCOs or QPOs alone (we have tested the limit of the

BH model). Furthermore, by connecting the theoretical results to observable astrophysical quantities, such as frequency modulations and energy amplification near the horizon, a bridge between nonlocal field corrections and high-energy phenomena in accreting BH systems is estabished. Although it builds upon the existing body of literature, the present study contributes a distinctive and comprehensive perspective on how nonlocal gravitational effects reshape the dynamics of matter and radiation in strong-field regimes to enrich both the phenomenology and theoretical landscape of modified gravity.

• The BH parameters derived from nonlocal gravity, in particular α and k, significantly influence the CME of particle collisions in the vicinity of the event horizon. As particles approach the horizon, the CME exhibits a rapid increase, which is characteristic of the strong gravitational field. However, the nonlocal corrections systematically modify this behavior. Higher values of k also lead to an enhancement of the CME, reflecting an effectively stronger gravitational interaction that increases the energy available in particle collisions. By contrast, larger values of α result in a suppression of the CME, which can be interpreted as a relative weakening of the gravitational effect because of nonlocal contributions. These parameters not only determine the maximum attainable collision energy but also affect the radial dependence of the CME near the horizon, demonstrating that even small deviations from the predictions of classical GR can produce observable effects in high-energy processes. This analysis emphasizes that nonlocal gravitational modifications are essential for understanding particle dynamics in strong-field regimes and may have measurable consequences for extreme astrophysical phenomena.

• The specific ranges of BH parameters (α,k) and particle parameters $(\mathcal{E},\mathcal{L})$ were selected to probe quantitatively the deviations from the Schwarzschild case while ensuring the existence of stable circular orbits outside the event horizon. Within these intervals, variations in (α) and (k) produced systematic modifications in the effective potential profile, leading to shifts in the ISCOs and changes in orbital stability criteria. In particular, increasing k generally results in a deeper potential well, thereby enhancing the CMEs of particle collisions near the horizon, whereas larger values of α tend to flatten the potential, reducing both CME and the binding energy of orbits. The chosen parameter ranges allow a controlled investigation of the quantitative influnece of nonlocal corrections on particle motion, stability thresholds, and energetic processes in the vicinity of the BH, providing a physically consistent framework for assessing deviations from classical GR.

VI. CONCLUSIONS

In this paper, the static, spherically symmetric BH geometry in nonlocal gravity extends the standard Schwarzschild solution by introducing additional correction terms in the metric functions $(h(r), f(r))$, governed by the parameters α and k. The function $h(r)$ retains the $-2/r$ dependence but acquires a new contribution proportional to $-\alpha/r^k$. The radial function $f(r)$ involves a more intricate modification encoded in $\mathcal{F}$, capturing the nonlocal character of the theory. These corrections remain small because α is assumed to be positive and much less than unity, and $k>1$ dictates the rate at which the modification decays with radial distance. In the limit $\alpha\to 0$, the Schwarzschild solution is exactly recovered, ensuring consistency with GR. The event horizon is no longer fixed at $r=2$ as in the classical case but shifts outward to $r_H = 2+\alpha/2^{k-1}$, showing that the presence of nonlocal corrections tends to enlarge the horizon. The influence of the parameters is twofold: α determines the strength of the deviation from the Schwarzschild geometry, and k controls how quickly these corrections fade at large distances. For values of k only slightly greater than one, the corrections extend further from the BH, whereas the higher value k confines them closer to the horizon. The analysis of the lapse function illustrates that both α and k contribute to an overall increase in its value, effectively reducing the gravitational redshift compared to the Schwarzschild case.

The analysis of particle dynamics around BHs in nonlocal gravity illustrates this structure in the motion of neutral test particles, which shows the influence of the BH parameters α and k. By taking the Hamiltonian formalism and testing the symmetries of the spacetime, the constants of motion (i.e., the specific energy and angular momentum) are derived and used to construct the effective potential and show the influence of BH parameters to illustrate the orbital behavior. The effective potential profiles illustrate that stable circular orbits correspond to their minima, whereas unstable orbits lie at the maxima, and the position of these extrema changes significantly with varying values of α and k. In particular, the effective potential grows stronger as either α or k increases, and the location of the stable orbits tends to move closer to the BH horizon, reflecting how nonlocal gravity corrections alter the usual Schwarzschild dynamics. The conditions for circular motion lead to explicit expressions for angular momentum and energy, whose graphical behaviors illustrate that angular momentum rises with increasing α but diminishes as k increases and the energy of circular orbits initially rises with α before decreasing for larger values, showing a nonmonotonic dependence. Both quantities exhibit growth with radial distance, consistent with the general relativistic picture. A particularly striking outcome arises in the study of ISCOs, where the combined conditions on the effective potential show that ISCO radii increase with α, implying that stronger nonlocal gravity effects push stable orbits outward, and they decrease with higher k, suggesting a competing effect that brings the ISCOs closer to the BH. This dual dependence shows the influnece of nonlocal gravity on particle dynamics, depending on the relation between α and k. The investigation of the effective force clarifies the nature of the gravitational interaction. For larger α, the force becomes more attractive, deepening the gravitational well. For larger k, the force tends toward repulsion, counteracting the attraction and modifying orbital stability.

The results of our analysis reveal several important features of oscillatory motion in nonlocal gravity; however, they also come with limitations that deserve attention. In the limit where parameters of nonlocal gravity vanish, i.e., $\alpha\to 0$ and $k\to 0$, our frequency expressions naturally reduce to the standard Schwarzschild case, reproducing well-known results for radial, latitudinal, and orbital frequencies in GR. This limit illustrates the consistency of the framework and shows that the observed deviations are entirely due to nonlocal modifications of gravity. In particular, the overlapping behavior of Ω_θ and Ω_ϕ persists in the Schwarzschild limit, and the radial frequency approaches the familiar form that determines the ISCOs at $r=6M$. Outside this limit, the presence of parameters α and k alters the stability regions significantly. Although α tends to push stable oscillatory orbits outward, effectively increasing the ISCO radius and enhancing precession effects, k pulls them inward, reducing the ISCOs and weakening periastron precession. Our treatment also assumes test particles without charge, spin, or self-gravity, restricting the analysis to neutral, spinless probes, which may not fully capture the behavior of realistic astrophysical matter in strong gravity. Additionally, we focused on equatorial plane perturbations and neglected higher-order nonlinear oscillations, meaning that our description is valid only for small perturbations around circular orbits. The nonlocal gravity model is parameterized phenomenologically through α and k. In future work, we plan to explore the full parameter space, including electromagnetic interactions or pressure effects from accreting matter, and compare the predicted frequency shifts directly with observational data from QPO measurements.

The study of the CME of colliding neutral test particles in the background of a nonrotating BH within nonlocal gravity reveals important insights into the energetic interactions near the horizon. As expressed in Fig. 9, the CME strongly depends on the BH parameters (α,k) and radial coordinate r. When the collision occurs near the event horizon, the CME exhibits a significant enhancement, reflecting the well-known Banãdos–Silk–West type effect in which the BH geometry acts as a natural particle accelerator. In the present case, nonlocal gravity modifications alter this behavior: increasing the parameter k enhances the CME, suggesting that stronger nonlocal contributions amplify the available energy in collisions, and higher values of α suppress the CME, indicating that the effective nonlocal potential acts as a regulating factor against unlimited energy growth. The radial behavior shows that as r increases, the CME decreases monotonically, approaching finite values at spatial infinity, which means that high-energy collisions are essentially confined to the near-horizon region. In the limiting case $r\to r_h$, the $\left(-\alpha r^{-k}-2/r+1\right)$ and (r^2) terms in the CME expression tend to be zero, potentially driving the CME to diverge under suitable conditions of particle energies and angular momenta. This divergence is controlled by the interplay of α and k, implying that although nonlocal gravity allows for high-energy collisions, it imposes bounds on the CME that are not present in the standard general relativistic case. In this context, the results indicate that nonlocal gravity significantly modifies the efficiency of BHs as particle properties and shows the influence of BH parameters.

In this study, the graphical analysis illustrates how the parameters of nonlocal gravity, that is, the coupling constant α and the fall-off parameter k, affect various physical quantities associated with BH spacetimes and test particle dynamics. Figure 1 illustrates the behavior of the lapse function $h(r)$ of a static, spherically symmetric BH in nonlocal gravity, where the influence of α and k is examined separately. In the left panel, $k=1.1$ is fixed while α is varied from 0.02 to 0.10. Increasing α enhances the value of $h(r)$ at any radial distance, effectively shifting the horizon radius outward and weakening the gravitational redshift relative to the Schwarzschild case. In the right panel, $\alpha=0.1$ is fixed and k is varied from 1.0 to 2.0. This leads to an increase in the lapse function as k increases, which corresponds to more localized corrections near the horizon. Figure 2 shows the effective potential $V_{\rm eff}(r)$ of the test particles, where the angular momentum is fixed at $\mathcal{L}=4$ and $\alpha=0.1$ in the left column. Varying k in the range $1.0\leqslant k\leqslant 2.0$, it is observed that the minima of the potential moves closer to the BH as k increases. The depth of the potential becomes more pronounced, indicating stronger binding and reduced orbital stability. In the right column, $\mathcal{L}=4$ and $k=1.1$ is fixed and α is varied between 0.02 and 0.10, showing a similar effect. A higher α increases the depth of the potential and shifts the stable orbits inward, demonstrating that nonlocal coupling enhances the gravitational pull. In Fig. 3, the angular momentum $\mathcal{L}$ of circular equatorial orbits is studied, with the left panel fixed at $k=0.1$ and varying α. It is shown that $\mathcal{L}$ increases with α, while the right panel is fixed at $\alpha=0.1$ with varying k. The angular momentum decreases as k increases in both cases. $\mathcal{L}$ also increases with the radial distance r, consistent with the expected centrifugal barrier. Figure 4 examines the specific energy $\mathcal{E}$ of particles in circular motion. In the left panel, $k=1.1$ is fixed and α is varied from 0.02 to 0.10; in the right panel, $\alpha=0.1$ is fixed and k ranges from 1.0 to 2.0. In both cases, energy initially increased and then decreased for larger values of α or k, reflecting the nontrivial interplay between gravitational attraction and nonlocal corrections, while $\mathcal{E}$ increased monotonically with r. Figure 5 shows the ISCO radius, where the $k=1.1$ on the left panel is fixed and α varies, leading to an outward shift of the ISCOs as α increases. In the right panel, $\alpha=0.1$ is fixed and increasing k results in a decrease of the ISCO radius. Thus, the coupling parameter α tends to destabilize orbits by pushing them outward, while higher k values improve stability by bringing the ISCOs closer to the horizon. Figure 6 plots the effective force acting on the test particles. In the left panel, $\mathcal{L}=3.5$ and $k=1.1$ are fixed and α increases from 0.02 to 0.10, showing that the force becomes more attractive with higher α. Conversely, in the right panel with fixed $\mathcal{L}=3.5$ and $\alpha=0.1$, increasing k from 1.0 to 2.0 produces a more repulsive force, highlighting the opposite roles played by the two parameters. Figure 7 presents the frequencies of harmonic oscillations, including radial (ν_r), latitudinal (ν_θ), and orbital (ν_ϕ), measured by a distant observer. The first row (left panel) corresponds to the Schwarzschild case $\alpha=0, k\approx 0$, providing a reference. Subsequent panels have fixed k and varying α, or fixed α and varying k. Evidently, increasing α shifts the frequency profiles outward, making the oscillations weaker and more extended, and increasing k shifts the profiles inward, compressing the oscillations closer to the horizon. Figure 8 studies the frequency of periastron precession Ω_P, where $k=1.1$ is fixed and α increases from 0.02 to 0.10 in the left panel, showing that Ω_P increases with α. In the right panel with fixed $\alpha=0.1$, varying k decreases the frequency of precession. In both cases, Ω_P decreases with the radial distance, consistent with weaker relativistic effects further from the BH. Figure 9 explores the CME of colliding particles. In the left panel with fixed $k=1.1$, increasing α decreases the CME. In the right panel with fixed $\alpha=0.1$, increasing k enhances the CME. In all cases, the CME grows near the horizon and decreases with radial distance, reflecting the fact that high-energy collisions are most efficient in the strong gravity region. These figures demonstrate that the nonlocal gravity parameters play complementary roles: α strengthens gravitational attraction, increases ISCO radius, enhances periastron precession, and reduces CME, while k tends to counteract by making forces more repulsive, reducing ISCOs, decreasing precession, and enhancing CME. Both parameters significantly reshape BH dynamics relative to the Schwarzschild case.

In the context of a nonrotating BH model, the logical and physical interpretation of the adopted nonlocal gravity framework gains particular importance as it allows us to isolate the influence of nonlocal corrections from rotational or charge-induced effects. This information also illustrates the fundamental structure of spacetime in this modified theory. From a logical standpoint, considering the static, spherically symmetric configuration ensures that the spacetime metric remains diagonal, with metric components depending solely on the radial coordinate. This symmetry simplifies the mathematical formulation and illustrates the essential features of gravitational attraction and horizon formation, allowing a direct comparison with the classical Schwarzschild BH solution. In the physical sense, the nonrotating, nonlocal BH represents a pure manifestation of how gravitational interactions are modified when the locality principle of GR is relaxed. The nonlocal parameters α and k show the physical meaning: α quantifies the strength of the deviation from local GR, encoding the amplitude of nonlocal field contributions, while k illustrates that these corrections diminish with radial distance, thus controlling the influence of spacetime interactions (testing the influence of BH parameters). As a result, the geometry no longer produces singularities identical to those of the Schwarzschild case because the nonlocal coupling acts as an effective regulator, softening curvature divergences near $r=0$ and shifting the event horizon outward to $r_H=2+\alpha/2k-1$. This result reveals an intriguing physical mechanism by which nonlocal effects may preserve causal structure while modifying the near-horizon regime. In the absence of angular momentum, nonlocal contributions still lead to measurable differences in gravitational redshift, effective potential depth, and orbital stability conditions, showing that the spacetime's causal and geodesic structure is intrinsically richer even without rotation. The logical consistency of this picture lies in the smooth limit $\alpha\to 0$, where the classical Schwarzschild solution is recovered, ensuring that nonlocal gravity naturally embeds GR as a low-energy effective limit. On physical grounds, this demonstrates that nonlocal gravity does not contradict the well-tested predictions of GR but rather extends them by incorporating scale-dependent corrections that manifest only in strong-field regions. The nonrotating BH in nonlocal gravity serves as the most transparent and theoretically robust laboratory to probe the physical implications of nonlocality, where one can distinctly trace how spacetime curvature, event horizons, and geodesic motion respond to a nonlocal gravitational field without the added complexity of frame-dragging or electromagnetic interactions. Such a setting provides not only logical clarity in the modeling of nonlocal effects but also physical credibility to the claim that the resulting geometry preserves essential GR features while subtly reshaping the strong-field behavior that could leave imprints on observational phenomena, such as orbital dynamics, QPOs, and energy extraction near the horizon.

ACKNOWLEDGMENTS

The authors sincerely thank the reviewer for their careful reading of the manuscript and for providing constructive comments and valuable suggestions, which have greatly improved the quality and clarity of this work.

References

[1] K. Akiyama *et al.* (Event Horizon Telescope Collaboration), Astrophys. J. Lett. **875**, L1 (2019)
[2] K. Akiyama *et al.* (Event Horizon Telescope Collaboration), Astrophys. J. Lett. **875**, L2 (2019)
[3] K. Akiyama *et al.* (Event Horizon Telescope Collaboration), Astrophys. J. Lett. **875**, L3 (2019)
[4] K. Akiyama *et al.* (Event Horizon Telescope Collaboration), Astrophys. J. Lett. **875**, L4 (2019)
[5] K. Akiyama *et al.* (Event Horizon Telescope Collaboration), Astrophys. J. Lett. **875**, L5 (2019)
[6] K. Akiyama *et al.* (Event Horizon Telescope Collaboration), Astrophys. J. Lett. **875**, L6 (2019)
[7] H. Falcke, F. Melia, and E. Agol, Astrophys. J. Lett. **528**, L13 (2000)
[8] F. Melia and H. Falcke, Annu. Rev. Astron. Astrophys. **39**, 309 (2001)
[9] M. Shahzadi, G. Lukes-Gerakopoulos, and M. Kološ, Phys. Rev. D **112**, 064013 (2025)
[10] M. Kološ, and M. Shahzadi, in Proceedings of RAGtime 23-25: Workshops on Black Holes and Neutron Stars **10**, 21 (2023)
[11] S. Iftikhar and M. Shahzadi, Eur. Phys. J. C **79**, 473 (2019)
[12] M. Shahzadi, Z. Yousaf, and S. U. Khan, Phys. Dark Univ. **24**, 100263 (2019)
[13] M. Kološ, M. Shahzadi, and A. Tursunov, Eur. Phys. J. C **83**, 323 ((2023)
[14] M. Shahzadi, M. Kološ, R. Saleem *et al.*, Phys. Rev. D **108**, 103006 (2023)
[15] M. Shahzadi, M. Kološ, R. Saleem *et al.*, Class. Quantum Grav. **41**, 075014 (2024)
[16] M. Sharif and M. Shahzadi, J. Exp. Theor. Phys. **127**, 491 (2018)
[17] M. Shahzadi, M. Kološ, Z. Stuchlík *et al.*, Eur. Phys. J. C **82**, 407 (2022)
[18] A. E. Broderick and A. Loeb, Mon. Not. Roy. Astron. Soc. **363**, 353 (2005)
[19] M. Moscibrodzka, C. F. Gammie, J. C. Dolence *et al.*, Astrophys. J. **706**, 497 (2009)
[20] J. Dexter, E. Agol, and P. C. Fragile, Astrophys. J. Lett. **703**, L142 (2009)
[21] A. E. Broderick, V. L. Fish, S. S. Doeleman *et al.*, Astrophys. J. **735**, 110 (2011)
[22] A. E. Broderick, T. Johannsen, A. Loeb *et al.*, Astrophys. J. **784**, 7 (2014)
[23] S. E. Gralla, D. E. Holz, and R. M. Wald, Rev. D **100**, 024018 (2019)
[24] R. Narayan, M. D. Johnson, and C. F. Gammie, Astrophys. J. Lett. **885**, L33 (2019)
[25] M. D. Johnson, and A. Lupsasca, Sci. Adv. **6**, eaaz1310 (2020)
[26] T. Bronzwaer, J. Davelaar, Z. Younsi *et al.*, Mon. Not. Roy. Astron. Soc. **501**, 4722 (2021)
[27] P. Kocherlakota *et al.* (Event Horizon Telescope Collaboration), Phys. Rev. D **103**, 104047 (2021)
[28] A. E. Broderick, P. Tiede, D. W. Pesce *et al.*, Astrophys. J. **927**(1), 6 (2022)
[29] T. Bronzwaer and H. Falcke, Astrophys. J. **920**(2), 155 (2021)
[30] M. Calzà, M. Rinaldi, and S. Vagnozzi, Phys. Rev. D **112**(10), 104055 (2025)
[31] M. Calzà, D. Pedrotti, G. W. Yuan *et al.*, Phys. Rev. D **112**, 124015 (2025)
[32] M. Calzà, D. Pedrotti, and S. Vagnozzi, Phys. Rev. D **111**(2), 024010 (2025)
[33] M. Calzà, D. Pedrotti, and S. Vagnozzi, Phys. Rev. D **111**, 024009 (2025)
[34] M. Calzà, F. Gianesello, M. Rinaldi *et al.*, Sci. Rep. **14**(1), 31296 (2024)
[35] M. Khodadi, S. Vagnozzi, and J. T. Firouzjaee, Sci. Rep. **14**(1), 26932 (2024)
[36] D. Pedrotti, and S. Vagnozzi, Phys. Rev. D **110**(8), 084075 (2024)
[37] S. Vagnozzi, R. Roy, Y. D. Tsai *et al.*, Class. Quant. Grav. **40**(16), 165007 (2023)
[38] Y. Chen, R. Roy, S. Vagnozzi *et al.*, Phys. Rev. D **106**(4), 043021 (2022)
[39] R. Roy, S. Vagnozzi, and L. Visinelli, Phys. Rev. D **105**(8), 083002 (2022)
[40] M. Khodadi, A. Allahyari, S. Vagnozzi *et al.*, JCAP **2020**(09), 026 (2020)
[41] S. Vagnozzi, C. Bambi, and L. Visinelli, Class. Quant. Grav. **37**(8), 087001 (2020)
[42] A. Allahyari, M. Khodadi, S. Vagnozzi *et al.*, JCAP **2020**(02), 003 (2020)
[43] S. Vagnozzi and L. Visinelli, Phys. Rev. D **100**, 024020 (2019)
[44] C. Bambi, K. Freese, S. Vagnozzi *et al.*, Phys. Rev. D **100**(4), 044057 (2019)
[45] S. Aktar, N. U. Molla, F. Rahaman *et al.*, JHEAp **47**, 100385 (2025)
[46] S. Kiroriwal, S. K. Maurya, J. Kumar *et al.*, Chin. J. Phys. **95**, 404 (2025)
[47] P. Mukherjee, U. Debnath, H. Chaudhary *et al.*, JCAP **2025**(05), 085 (2025)
[48] Y. Pahlavon, F. Atamurotov, A. Bouzenada *et al.*, Nucl. Phys. B **1014**, 116882 (2025)
[49] H. Chaudhary, U. Debnath, S. K. Pacif *et al.*, Ann. Phys. **537**(5), 2400421 (2025)
[50] X. Wang, W. Lin, G. Mustafa *et al.*, Phys. Rev. D **111**(8), 084009 (2025)
[51] S. K. Maurya, A. Errehymy, K. N. Singh *et al.*, JCAP **2025**(04), 004 (2025)
[52] G. Rakhimova, F. Abdulkhamidov, F. Atamurotov *et al.*, Chin. J. Phys. **94**, 66 (2025)
[53] G. Fatima, T. Zhu, F. Javed *et al.*, Eur. Phys. J. C **85**(2), 208 (2025)
[54] G. Fatima, F. Javed, A. Waseem *et al.*, Phys. Dark Universe **47**, 101820 (2025)
[55] F. Javed, S. Shaukat, G. Mustafa *et al.*, Phys. Dark Universe **47**, 101826 (2025)
[56] G. Mustafa, F. Javed, S. K. Maurya *et al.*, Phys. Dark

Universe **47**, 101825 (2025)
[57] N. U. Molla, H. Chaudhary, S. Capozziello *et al.*, Phys. Dark Universe **47**, 101804 (2025)
[58] G. Fatima, F. Javed, G. Mustafa *et al.*, Int. J. Geom. Meth. Mod. Phys. **22**(02), 2450279 (2025)
[59] H. Chaudhary, S. K. J. Pacif, G. Mustafa *et al.*, JHEAp **45**, 340 (2025)
[60] A. Ditta, G. Mustafa, and A. Mahmood, JHEAp **45**, 350 (2025)
[61] G. Mustafa, S. K. Maurya, T. Naseer *et al.*, Nucl. Phys. B **1012**, 116812 (2025)
[62] B. Rasheed, A. Ditta, T. Naseer *et al.*, Int. J. Geom. Meth. Mod. Phys. **22**(04), 2450302 (2025)
[63] M. K. Jasim, S. K. Maurya, S. Ray *et al.*, Int. J. Geom. Meth. Mod. Phys. **22**, 2550123 (2025)
[64] A. Hussain, F. Javed, G. Fatima *et al.*, Int. J. Geom. Meth. Mod. Phys. **22**(03), 2450297 (2025)
[65] N. Arkani-Hamed, S. Dimopoulos, G. Dvali *et al.*, arXiv: hep-th/0209227
[66] S. Nojiri and S. D. Odintsov, Phys. Lett. B **659**, 821 (2008)
[67] G. Calcagni, M. Montobbio, and G. Nardelli, Phys. Rev. D **76**, 126001 (2007)
[68] T. Biswas, E. Gerwick, T. Koivisto *et al.*, Phys. Rev. Lett. **108**, 031101 (2012)
[69] S. Park and S. Dodelson, Phys. Rev. D **87**, 024003 (2013)
[70] M. Maggiore and M. Mancarella, Phys. Rev. D **90**, 023005 (2014)
[71] Y. Dirian, S. Foffa, N. Khosravi *et al.*, JCAP **06**, 033 (2014)
[72] S. Capozziello, R. D'Agostino, and O. Luongo, Phys. Lett. B **834**, 137475 (2022)
[73] C. Deffayet and R. P. Woodard, JCAP **05**, 042 (2024)
[74] L. Modesto, Phys. Rev. D **86**, 044005 (2012)
[75] L. Modesto and L. Rachwał, Int. J. Mod. Phys. D **26**, 1730020 (2017)
[76] S. Deser and R. P. Woodard, Phys. Rev. Lett. **99**, 111301 (2007)
[77] E. Belgacem, A. Finke, A. Frassino *et al.*, JCAP **02**, 035 (2019)
[78] S. Deser and R. P. Woodard, JCAP **06**, 034 (2019)
[79] J. C. Ding and J. B. Deng, JCAP **12**, 054 (2019)
[80] C. Y. Chen, P. Chen, and S. Park, Phys. Lett. B **796**, 112 (2019)
[81] D. Jackson and R. Bufalo, JCAP **05**, 043 (2022)
[82] S. Capozziello and R. D'Agostino, Phys. Dark Univ. **42**, 101346 (2023)
[83] D. Jackson and R. Bufalo, JCAP **05**, 010 (2023)
[84] C. Y. Chen and S. Park, Phys. Rev. D **103**, 064029 (2021)
[85] A. Kehagias and M. Maggiore, JHEP **08**, 029 (2014)
[86] G. Calcagni, L. Modesto, and Y. S. Myung, Phys. Lett. B **783**, 19 (2018)
[87] U. Kumar, S. Panda, and A. Patel, Eur. Phys. J. C **80**, 614 (2020)
[88] L. Buoninfante, B. L. Giacchini, and T. de Paula Netto, arXiv: 2211.03497 [gr-qc]
[89] R. D'Agostino and V. De Falco, Phys. Rev. D **112**(6), 064028 (2025)
[90] J. Rayimbaev, P. Tadjimuratov, A. Abdujabbarov *et al.*, Galaxies **9**(4), 75 (2021)
[91] S. Jumaniyozov, M. Zahid, M. Alloqulov *et al.*, Eur. Phys. J. C **85**, 126 (2025)
[92] S. Faraji, Astron. Rep. **67**, S207 (2023)
[93] Z. Stuchlík and J. Vrba, JCAP **2021**(11), 059 (2021)
[94] J. Homan, M. Klein-Wolt, S. Rossi *et al.*, Astrophys. J. **586**, 1262 (2003)
[95] J. Rayimbaev, B. Ahmedov, and A. H. Bokhari, Int. J. Mod. Phys. D **31**, 2240004 (2022)
[96] M. Qi, J. Rayimbaev, and B. Ahmedov, Eur. Phys. J. C **83**, 730 (2023)
[97] L. Rezzolla, and O. Zanotti, *Relativistic Hydrodynamics* (2013)
[98] L. Rezzolla, S. Yoshida, T. J. Maccarone *et al.*, Mon. Not. R. Astron. Soc. **344**, L37 (2003)
[99] G. Torok, A. Kotrlova, E. Sramkova *et al.*, Astron. Astrophys. **531**, A59 (2011)
[100] Z. Stuchlik, A. Kotrlova, and G. Torok, Astron. Astrophys. **525**, A82 (2011)
[101] Z. Stuchlik, A. Kotrlova, and G. Torok, Astron. Astrophys. **552**, A10 (2013)
[102] G. Mustafa, I. Hussain, and W. M. Liu, Chin. J. Phys. **80**, 148 (2022)
[103] X. Jiang, P. Wang, H. Yang *et al.*, Eur. Phys. J. C **81**, 1043 (2021)
[104] L. Amarilla, E. F. Eiroa, and G. Giribet, Phys. Rev. D **81**, 124045 (2010)
[105] Y. Liu, G. Mustafa, S. K. Maurya *et al.*, Eur. Phys. J. C **83**, 584 (2023)
[106] Z. Stuchlík and M. Kološ, Astron. Astrophys. **586**, A130 (2016)
[107] R. A. Remillard, J. E. McClintock, G. J. Sobczak *et al.*, Astrophys. J. **517**(2), L127 (1999)
[108] E. H. Morgan, R. A. Remillard, and J. Greiner, Astrophys. J. **482**(2), 993 (1997)
[109] R. A. Remillard, J. E. McClintock, J. A. Orosz *et al.*, Astrophys. J. **637**(2), 1002 (2006)
[110] S. Jumaniyozov, Eur. Phys. J. C **85**, 1267 (2025)
[111] O. Donmez, Eur. Phys. J. C **84**(5), 524 (2024)
[112] A. Garg, R. Misra, and S. Sen, Mon. Not. R. Astron. Soc. **514**(3), 3285 (2022)
[113] M. Masterson, E. Kara, C. Panagiotou *et al.*, Nature **638**, 370 (2025)
[114] C. Bambi, JCAP **2012**(09), 014 (2012)
[115] F. Abdulkhamidov, B. Narzilloev, I. Hussain *et al.*, Eur. Phys. J. C **84**(4), 420 (2024)
[116] G. Török, Astron. Nachr. **326**(9), 856 (2005)
[117] J. Petri, Astrophys. Space Sci. **318**(3), 181 (2008)
[118] F. Vignarca, S. Migliari, T. Belloni *et al.*, Astron. Astrophys. **397**(2), 729 (2003)
[119] D. R. Pasham, S. B. Cenko, A. Zoghbi *et al.*, Astrophys. J. Lett. **811**(1), L11 (2015)
[120] R. V. Wagoner, Astrophys. J. Lett. **752**(2), L18 (2012)
[121] G. Mustafa, E. Demir, A. Davlataliev *et al.*, Phys. Dark Univ. **46**, 101644 (2024)
[122] J. Rayimbaev, S. Murodov, A. Shermatov *et al.*, Eur. Phys. J. C **84**(10), 1114 (2024)
[123] O. Dönmez, Astrophys. Space Sci. **293**, 323 (2004)
[124] P. J. Montero and O. Zanotti, Mon. Not. Roy. Astron. Soc. **419**, 1507 (2011)
[125] Z. Stuchlík, M. Kološ, and A. Tursunov, Publ. Astron. Soc. Jpn. **74**, 1220 (2022)
[126] K. Boshkayev, O. Luongo, and M. Muccino, Phys. Rev. D **108**, 124034 (2023)
[127] K. Boshkayev, T. Konysbayev, Y. Kurmanov *et al.*, Mon. Not. Roy. Astron. Soc. **531**, 3876 (2024)
[128] K. Boshkayev, A. Idrissov, O. Luongo *et al.*, Phys. Rev. D **108**, 044063 (2023)

[129] S. Mitra, J. Vrba, J. Rayimbaev *et al*., Phys. Dark Univ. **46**, 101561 (2024)
[130] J. Rayimbaev, U. Eshimbetov, B. Majeed *et al*., Chin. Phys. C **48**, 055104 (2024)
[131] F. Abdulkhamidov, P. Nedkova, J. Rayimbaev *et al*., Phys. Rev. D **109**, 104074 (2024)
[132] J. Rayimbaev, A. Abdujabbarov, F. Abdulkhamidov *et al*., Eur. Phys. J. C **82**, 1110 (2022)
[133] Z. Stuchlík, A. Kotrlová, *in RAGtime 8/9: Workshops on Black Holes and Neutron Stars* (2007).
[134] Z. Stuchlík and A. Kotrlová, Gen. Relativ. Gravit. **41**, 1305 (2009)
[135] S. Murodov, K. Badalov, J. Rayimbaev *et al*., Symmetry **16**, 109 (2024)
[136] S. Murodov, J. Rayimbaev, B. Ahmedov *et al*., Symmetry **15**, 2084 (2023)
[137] U. Nucamendi, R. Becerril, and P. Sheoran, Eur. Phys. J. C **80**, 35 (2020)
[138] A. N. Aliev and P. Talazan, Phys. Rev. D **80**, 044023 (2009)
[139] K. Jusufi, M. Jamil, and P. H. R. S. Moraes, Eur. Phys. J. C **80**, 354 (2020)
[140] S. Das and E. C. Vagenas, Can. J. Phys. **87**, 233 (2009)
[141] K. Jusufi, M. Azreg-Aïnou, M. Jamil *et al*., Int. J. Geom. Meth. Mod. Phys. **19**, 2250068 (2022)
[142] J. Abedi, H. Arfaei, J. Cosmol. Astropart. Phys. **2016**, 042 (2016)
[143] I. Banerjee, J. Cosmol. Astropart. Phys. **08**, 034 (2022)
[144] S. E. Motta and T. M. Belloni, Astron. Astrophys. **684**, A209 (2024)
[145] C. Y. Shao, C. Zhang, W. Zhang *et al*., Phys. Rev. D **109**, 064012 (2024)
[146] K. Nozari and M. Shoukrani, Astrophys. Space Sci. **339**, 111 (2012)
[147] P. Nicolini, Int. J. Mod. Phys. A **24**, 1229 (2009)
[148] J. Rayimbaev, A. H. Bokhari, and B. Ahmedov, Class. Quant. Grav. **39**, 075021 (2022)
[149] A. Ashraf, A. Bouzenada, S. K. Maurya *et al*., Phys. Dark Univ. **47**, 101787 (2025)
[150] G. Mustafa, P. Channuie, F. Javed *et al*., Phys. Dark Univ. **47**, 101765 (2025)
[151] G. Mustafa, S. K. Maurya, P. Channuie *et al*., Phys. Dark Univ. **47**, 101753 (2025)
[152] A. Ashraf, A. Ditta, A. Bouzenada *et al*., Phys. Dark Univ. **48**, 101836 (2025)
[153] A. Ashraf, A. Ditta, A. Bouzenada *et al*., Phys. Dark Univ. **47**, 101823 (2025)
[154] A. Ditta, A. Bouzenada, G. Mustafa *et al*., Phys. Dark Univ. **47**, 101818 (2025)
[155] A. Ditta, A. Bouzenada, G. Mustafa *et al*., Phys. Dark Univ. **46**, 101573 (2024)
[156] A. Bouzenada, A. Ditta, A. Ashraf *et al*., Nucl. Phys. B **1017**, 116928 (2025)
[157] A. Saleem, A. Ditta, A. Bouzenada *et al*., Nucl. Phys. B **1017**, 116926 (2025)
[158] S. K. Maurya, A. Ditta, A. Bouzenada *et al*., Nucl. Phys. B **1020**, 117139 (2025)
[159] A. Ditta, A. Bouzenada, M. Alomar *et al*., Nucl. Phys. B **1019**, 117099 (2025)
[160] B. Turimov, S. Usanov, and Y. Khamroev, Phys. Dark Univ. **48**, 101876 (2025)